Chapter 7
Power Flow Analysis and Reactive Power Compensation of Grid Connected Wind Energy Conversion Systems

J. Ravishankar

Abstract The power flow analysis is the basic tool for analyzing the steady state operation of any power system. It also provides the necessary initial conditions to investigate the dynamic performance of the system. This chapter discusses the power flow analysis of grid connected wind energy conversion systems (WECS). The power flow analysis with WECS is quite complicated, unlike the analysis with conventional sources, because: 1. The power injected into the grid by WECS depends on the instantaneous wind speed, which varies unpredictably. 2. Most WECS use induction generators. Therefore, the operating slip of the machine has to be determined. The machine operates at a slip for which the mechanical power developed by the turbine is equal to the electrical power developed by the induction generator. This chapter outlines two methods (1) sequential method of power flow and (2) simultaneous method of power flow analysis for grid connected WECS. Both the methods of power flow are tested on a sample system and the results are presented. This chapter also looks into the effect of various types of reactive power compensation, namely, shunt, series and series-shunt compensation, on the steady state performance of WECS equipped with squirrel-cage induction generators. A cost effective method to strengthen the given network between the point of common coupling (PCC) and rest of the grid is proposed. The effect of compensation in improving the penetration level of wind energy into the grid is also analyzed.

Keywords Wind energy · Induction generators · Point of common coupling · Power flow analysis · Reactive power compensation

J. Ravishankar (✉)
School of Electrical Engineering and Telecommunications, The University of New South Wales, Sydney, NSW 2052, Australia
e-mail: jayashri.ravishankar@unsw.edu.au

J. Hossain and A. Mahmud (eds.), *Renewable Energy Integration*,
Green Energy and Technology, DOI: 10.1007/978-981-4585-27-9_7,
© Springer Science+Business Media Singapore 2014

7.1 Introduction

One of the most critical issues for wind energy exploitation in developing countries like India has been the transmission capacity of the grid in the areas where the wind farms exist. Wind farms are concentrated in the rural areas where the existing transmission grids are very weak. In addition, the wind farms were developed during a comparatively short period of time in a few areas, and the reinforcement of the transmission systems in these areas has lagged behind the fast development of wind energy [1].

One of the problems with wind energy generation is the dependence of the injected power on the wind speed. The wind speed cannot be predicted, but the probability of a particular wind speed occurring can be estimated. This can be done by assuming a Weibull or a Rayleigh probability distribution. Once the wind speed is known, the power injected into the grid can be calculated by means of the wind turbine power curve. Therefore, assessment of steady state performance of electrical networks with WECS is not as simple as with conventional generation and can be planned from a probabilistic point of view only.

Most WECS are equipped with induction generators. Early systems used squirrel-cage generators as fixed-speed types and the current systems use doubly-fed induction generators (DFIG) that are capable of producing a variable-speed operation. For the dynamic analysis of a system, correct initialization is required otherwise time will be wasted as the system tries to find a steady-state operating point as the initial condition [2]. Initializing most components' variables is a straightforward, direct process. However, initializing induction machine variables requires an indirect, iterative process [3]. Therefore, the power flow analysis in systems with induction machines needs additional iterative procedure.

Several attempts have been made in the past to investigate the steady state behaviour of induction machines in a wind farm [4–9]. All these attempts involve a sequential approach to calculate the state variables of the wind generators. This sequential iterative approach is rather attractive because it is straightforward to implement in existing power flow programs, but caution has to be exercised because it will yield no quadratic convergence [10], and an additional set of nonlinear algebraic equations have to be solved to obtain the values of the wind generator's state variables [11, 12].

In this Chapter, the power flow of a radial system with WECS is simulated, using two methods (a) sequential and (b) simultaneous method of power flow. The WECS is modeled with squirrel-cage induction generators. Simulation carried out on a 9-bus radial system shows that the power flow results of both the methods are comparable. Additionally, the simultaneous method of power flow analysis exhibits better convergence characteristics.

From the power flow results, it is observed that the grid connected induction generator imports heavy reactive power from the grid, resulting in poor power factor and reducing the voltage at the WECS terminals. Therefore, reactive power support is needed at WECS terminals for voltage regulation and improvement of low voltage ride-through capabilities. As the wind speed continuously changes, the

voltage at the PCC fluctuates. A possible way to improve this situation is by incorporating reactive power compensation. Simulation results show that the combination of series and shunt compensation results in a very good voltage profile at PCC and a significant reduction in transmission line current due to the reduction of reactive power flow through the line. This also allows more turbines to be connected at the PCC.

7.2 Steady State Model of Induction Generator

For power flow analysis, the induction generator can be represented by the well-known equivalent circuit shown in Fig. 7.1.

In Fig. 7.1, R_s—stator resistance, R_r—rotor resistance, X_s—stator leakage reactance, X_r—rotor leakage reactance, X_m—magnetizing reactance, $\bar{I}_1$—stator current, $\bar{I}_2$—rotor current, $\overline{V}$—terminal voltage, s—slip given by $(\omega_s\text{-}\omega_r)/\omega_s$.

From Fig. 7.1, the current I_1 can be written as,

$$\bar{I}_1 = \frac{\bar{V}}{(R_s + R_e) + j(X_s + X_e)} \tag{7.1}$$

where,

$$R_e + jX_e = \frac{jX_m\left(\frac{R_r}{s} + jX_r\right)}{\frac{R_r}{s} + j(X_m + X_r)} \tag{7.2}$$

The per-unit active power transferred from the rotor to the stator through the air gap, called air gap power, is readily calculated from the equivalent circuit as,

$$P_g = I_2^2 \frac{R_r}{s} \tag{7.3}$$

The electrical power developed in the rotor is,

$$P_e = I_2^2 \frac{R_r}{s}(1 - s) \tag{7.4}$$

where the slip is negative. The electrical torque developed is then given by,

$$\tau_e(V, s) = \frac{V^2 X_m^2 \frac{R_r}{s}}{\left[\left(R_x + \frac{R_r}{s}\right)^2 + (X_x + X_r)^2\right]\left[R_s^2 + (X_s + X_m)^2\right]} \tag{7.5}$$

where

$$R_x + jX_x = \frac{jX_m(R_s + jX_r)}{R_s + j(X_s + X_m)} \tag{7.6}$$

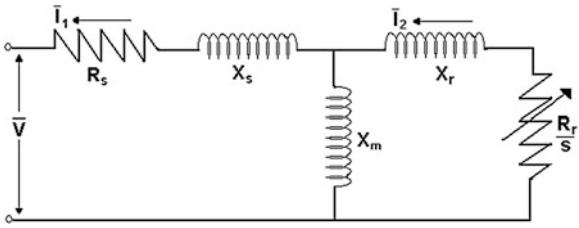

Fig. 7.1 Steady state equivalent circuit of induction generator

7.3 Turbine Aggregation

It is possible to aggregate the machines in the wind farm, consisting of N parallel turbines, by a single machine equivalent with a re-scaled power capacity. The following are valid:

- The wind turbines are identical, including the parameters of the generator used.
- Wind speeds at the wind farm are uniform.
- Each wind turbine runs at the same operating condition at all times. Thus the voltage, current and power of each wind turbine are identical.
- With the aggregation procedure, the equivalent wind turbine of the entire wind farm is a scale up of a single wind turbine, i.e. the base power becomes N times the base power of a single wind turbine in the farm.
- Similarly, the equivalent generator impedance becomes 1/N times the impedance of the generator in the individual turbine.

In this Chapter, the single machine equivalent is applied and found to reduce the computational time.

7.4 Power Flow Analysis

In steady state, the induction generator is modeled based on the following two facts [13]:

(i) The machine can be simulated in steady state as impedance if its parameters and slip are known.

(ii) The slip of the machine can be calculated if its power coefficient curve and wind speed are known.

When a wind farm with asynchronous generation is included in the power flow analysis, the PQ and RX [14, 15] buses are the most commonly used. DFIG machines can be modeled as PV buses, however, handling this is not always easy especially when multiple and different types are combined [16]. When the conventional PQ bus model is used, the real and reactive powers have constant values, although these values can be modified in order to represent loads depending either on the voltage or on the frequency [17].

7.4.1 Sequential Method of Power Flow Analysis

In the sequential method, for a given wind speed and a given rotor speed the power extracted from the WECS is calculated from power coefficient curve. To the same rotor speed, the power developed by the induction generator is calculated from the results of power flow analysis. These two powers are then compared for convergence. Thus, in this method power flow analysis is carried out for every value of calculated slip. The analysis is continued until the operating slip is obtained.

The algorithmic steps for the sequential solution method for a given wind speed, are presented below:

1. Begin with a slip $s = s_{rated}$. With this value of s, calculate the impedance Z of the induction generator.
2. With these values, model the wind farm as impedance by including the admittance of the generators in the admittance matrix.
3. Run the power flow and obtain the solution. With these results, calculate power developed by the generator by using Eq. (7.4).
4. With the value of s, assumed in the step 1, calculate the tip-speed ratio, C_p and power extracted from the wind using Eqs. (7.7), (7.8) and (7.10) respectively. The tip-speed ratio is given by,

$$\lambda = \frac{\omega R}{v} \tag{7.7}$$

The power coefficient is computed using,

$$C_p(\lambda, \theta) = C_1\left(C_2 \frac{1}{\Lambda} - C_3\theta - C_4\theta^x - C_5\right)e^{\left(-C_6\frac{1}{\Lambda}\right)} \tag{7.8}$$

where

$$\frac{1}{\Lambda} = \frac{1}{\lambda + 0.008\theta} - \frac{0.035}{1 - \theta^3} \tag{7.9}$$

and C_1 to C_6, x are constants. The power extracted from the turbine is then,

$$P_t = C_P \times \frac{1}{2}\rho A v^3 \tag{7.10}$$

where, ρ is the density of dry air, v is the speed of the wind in m/s and A is the swept area of the blades in m^2

5. Compute $\Delta P_m = P_t - P_e$. If $|\Delta P_m| >$ Specified tolerance value, ε, then update the slip by using, $s^{new} = s + \Delta s$ and go to Step 2. Else stop the process.

Here, $\Delta s = -J^{-1} * \Delta P_m$, where the Jacobian J is given by,

$$J = \frac{\partial(P_t(s) - P_m(s))}{\partial s} \tag{7.11}$$

7.4.2 Simultaneous Method of Power Flow Analysis

This method determines simultaneously the state variables corresponding to nodal voltage magnitudes and angles of the network and slip of induction generators [18]. In this method, the WECS is modeled as a variable PQ bus. Assuming adequate initial conditions, the method retains Newton's quadratic convergence. In this method the N-R power flow algorithm is reformulated to include the mismatch equation ΔP_m. The unified power flow formulation is,

$$\begin{bmatrix} [\Delta P] \\ [\Delta Q] \\ [\Delta P_m] \end{bmatrix} = \begin{bmatrix} \left[\frac{\partial P}{\partial \theta}\right] & \left[|V|\frac{\partial P}{\partial |V|}\right] & \left[\frac{\partial P}{\partial s}\right] \\ \left[\frac{\partial Q}{\partial \theta}\right] & \left[|V|\frac{\partial Q}{\partial |V|}\right] & \left[\frac{\partial Q}{\partial s}\right] \\ \left[-\frac{\partial \Delta P_m}{\partial \theta}\right] & \left[-|V|\frac{\partial \Delta P_m}{\partial |V|}\right] & \left[-\frac{\partial \Delta P_m}{\partial s}\right] \end{bmatrix} \times \begin{bmatrix} [\Delta \theta] \\ [\Delta |V|/|V|] \\ [\Delta s] \end{bmatrix} \tag{7.12}$$

where $\left[\frac{\partial \Delta P_m}{\partial S}\right]$ is a diagonal matrix whose order is equal to the number of wind farms in the network. Their elements are given by,

$$\frac{\partial \Delta P_m}{\partial s} = \frac{1}{2}\rho a v^3 [C_2 - EC_1] C_1 e^{C_6 \Lambda} \frac{\omega r/v}{D} + \frac{A}{sC^2}(B - C) \tag{7.13}$$

where the values of A to E are given by,

$$A = \frac{V^2 X_m^2 R_r/s}{R_s^2 + (X_s + X_m)^2} \tag{7.14}$$

$$B = \frac{2R_r}{s}\left(R_x + \frac{R_r}{s}\right) \tag{7.15}$$

$$C = \left(R_x + \frac{R_r}{s}\right)^2 + (X_x + X_r)^2 \tag{7.16}$$

$$D = (\lambda + 0.08\theta)^2 \tag{7.17}$$

$$E = C_2 \Lambda - C_3 \theta - C_5 \tag{7.18}$$

Here, ΔP_m is the difference between the power extracted from the turbine and electrical power developed in the machine and Δs is the vector of incremental changes in induction generator's slip. It is to be noted that when the induction machine slip varies, its generated electrical power varies. This in-turn impacts the mismatch vector ΔP_m. Thus, Δs has a significant influence on the power flow result.

In the above unified power flow Eq. (7.12) the dimension of the Jacobian for the power system having N_g generator buses, N_l load buses and N_w wind farm buses with induction generators is $(N_g + 2N_l + 3N_w - 1)$ x $(N_g + 2N_l + 3N_w - 1)$.

7.4.3 Convergence Characteristics of Simultaneous and Sequential Methods of Power Flow

Both the methods of power flow are tested on a 9-bus radial system given in Fig. 7.2 [19]. The data for the same is provided in Appendix I.

Simulations are carried out for wind speeds ranging from 5 m/s (cut-in speed) to 25 m/s (cut-out speed) in steps of 2 m/s and with one turbine connected at bus 9. It should be noted that the ideal location of the WECS is identified to be at bus 9, by running power flow simulations with WECS at buses 2, 7, 8 and 9. Voltage magnitudes of all the buses and power system losses of each case were compared and it was noted that WECS interconnected at bus 9, produced the best voltage magnitude and minimum losses. The variation of voltage at the WECS terminals (bus 9), real power generated and reactive power consumed by the WECS using the simultaneous and sequential methods of power flow are presented in Table 7.1. For the system considered, the Jacobian matrix for the simultaneous method is a (17×17) matrix. The elements of the Jacobian are given in Appendix II.

The analysis reveals that the results obtained in both methods are comparable. It is also observed that the number of iterations with sequential method is 20 (5 times power flow $\times$ 4 iterations in every power flow), whereas with simultaneous method it is only 6. Thus the convergence with simultaneous method is better.

In Table 7.1, P is the power generated at WECS terminals (measured at bus 9), Q is the reactive power consumed by WECS, V and δ represent the voltage magnitude and phase angles of bus 9.

7.5 Grid Strengthening

The number of wind turbines on-line determines the loading of the transmission system. Thus, it affects the voltage at the WECS terminals. To illustrate this, the simulation is initially run for one wind turbine connected at bus 9. The wind turbines considered are uncompensated. Repeated runs are performed by increasing the number of turbines connected at bus 9. In the simulation, the impedance of induction generators connected at bus 9 is calculated as Z/N, where N is the number of turbines. The plots of voltage at WECS terminals, real power generated and reactive power consumed by WECS, for wind speeds ranging from 5 m/s to 25 m/s, obtained through simulation are given in Figs. 7.3, 7.4 and 7.5 respectively. It is clear that as the number of turbines increases, the reactive power consumed increases and as a result the voltage drops. These are reflected in Figs. 7.5 and 7.3.

As more turbines are connected, the generated power increases as illustrated in Fig. 7.4. But when the number of wind turbines connected is more than 2, the aerodynamic power of the wind turbine over-powers the power developed by induction generator and thus the wind turbine goes into a runaway condition. This is

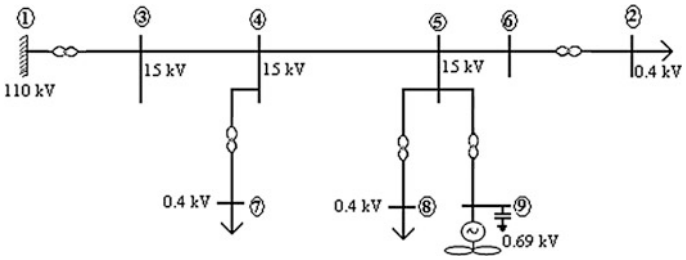

Fig. 7.2 Single-line diagram of 9-bus radial system

Table 7.1 Power flow results of 9-bus radial system for bus 9

Wind Speed (m/s)	Sequential method				Simultaneous method			
	V (PU)	δ (deg)	P (kW)	Q (kVAR)	V (PU)	δ (deg)	P (kW)	Q (kVAR)
5	0.9787	0.9278	82.9141	214.6557	0.9780	0.9047	82.8858	213.6035
7	0.9843	1.9068	211.1735	221.9829	0.9838	1.8937	211.1126	223.4978
9	0.9895	3.4596	367.4732	241.6829	0.9890	3.1213	367.5418	242.8460
11	0.9918	4.6453	517.8517	263.7065	0.9922	4.3267	517.4311	264.0342
13	0.9927	5.3267	636.3004	289.5034	0.9933	5.3135	636.7911	291.5365
15	0.9927	5.9654	715.0093	309.2507	0.9934	5.9736	714.7080	310.7337
17	0.9928	6.2827	750.0036	325.7328	0.9932	6.2816	750.0001	325.8205
19	0.9928	6.2826	749.2659	318.9891	0.9932	6.2749	749.6892	318.5931
21	0.9928	6.2839	720.8318	310.4878	0.9933	6.2748	720.6771	310.3805
23	0.9928	5.7648	672.8567	301.7757	0.9934	5.6124	672.2771	302.4401
25	0.9925	5.2987	612.9106	289.0685	0.9932	5.1093	612.3689	289.6878

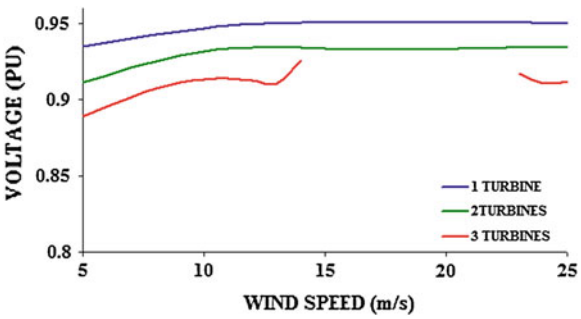

Fig. 7.3 Effect of increasing the connected wind turbines on voltage at WECS terminals

reflected by the non-convergence of the power flow in the operating wind speed region considered (shown by red line in Figs. 7.3, 7.4 and 7.5).

The discontinuity of the curve (red line) can be explained as follows. The induction generator operates at a slip where the aerodynamic power equals the electrical power developed. When the number of turbines connected at the PCC increases to 3, the aerodynamic power increases 3 fold. Correspondingly, with 3

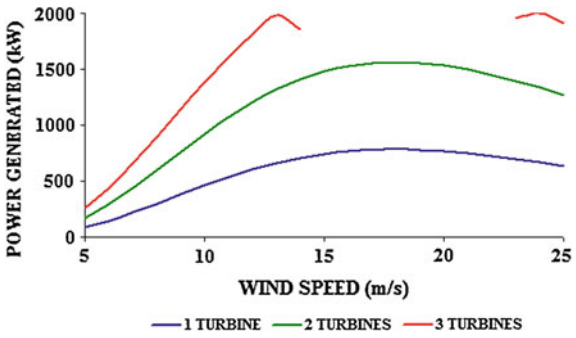

Fig. 7.4 Effect of increasing the connected wind turbines on real power generated by WECS

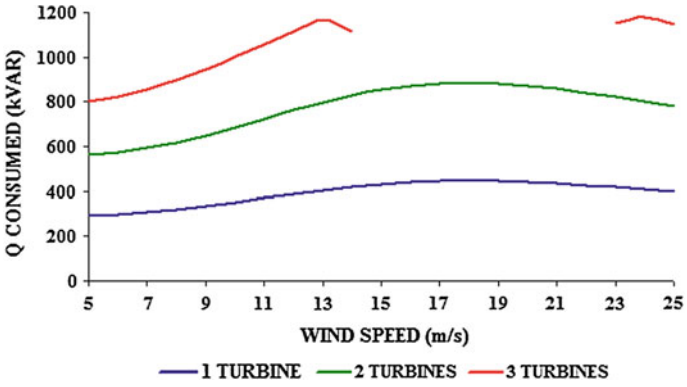

Fig. 7.5 Effect of increasing the connected wind turbines on reactive power consumed by WECS

induction generators in parallel, the electrical power developed should also increase. At the same time, due to the nature of induction machines, the Q consumed by WECS also increases. This decreases the voltage at the PCC, which in-turn reduces the power generated. This results in a condition where the aerodynamic power is much greater than the electrical power. Thus, it is clear that the considered 9-bus radial system cannot accommodate more than two turbines.

To meet the demand of increased power production from wind, more wind turbines are required to be connected to the wind farms. Therefore, the grid needs to be strengthened to accommodate more turbines. Figures 7.6, 7.7 and 7.8 respectively give the voltage at WECS terminals, real power generated and reactive power consumed by the WECS after strengthening of the transmission line between the PCC (bus 5 in Fig. 7.2) and bus 3 in Fig. 7.2. It is observed that when a double circuit line is used, 5 uncompensated wind turbines can be connected. The power flow converges for all wind speeds in the range, i.e., from cut-in to cut-out speeds. As the effective line impedance between the PCC and the grid is now reduced by half, the grid becomes stiffer. As seen in Fig. 7.8, obviously the

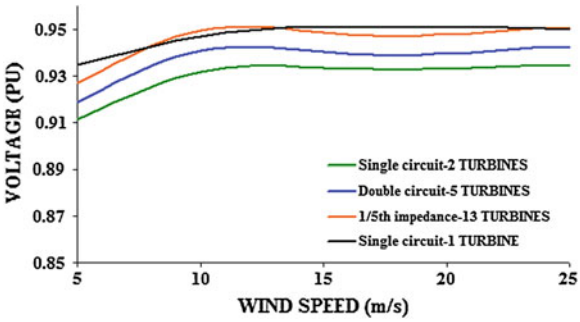

Fig. 7.6 Grid strengthening—Voltage at WECS terminals

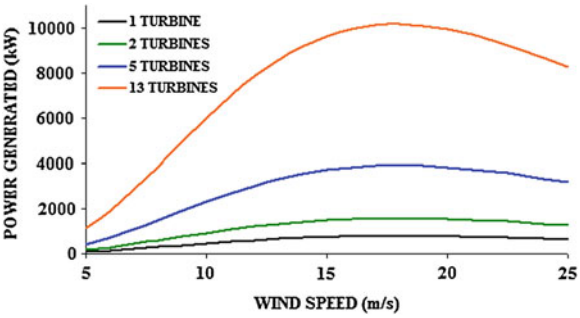

Fig. 7.7 Grid strengthening—Real power generated by WECS

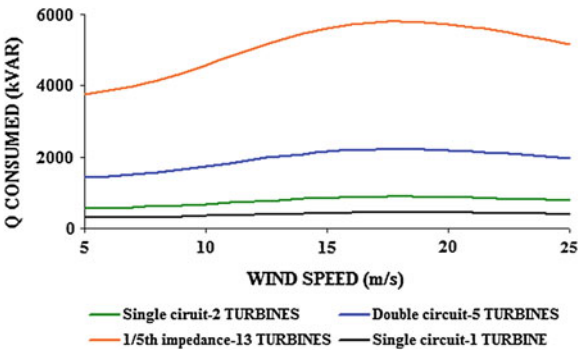

Fig. 7.8 Grid strengthening—Reactive power consumed by WECS

reactive power drawn from the grid increases, but at the same time the voltage at WECS terminals also increases as seen in Fig. 7.6. This increase in voltage results from grid strengthening. When the grid is further strengthened by reducing the impedance of the transmission line 5 times, 13 uncompensated wind turbines can be connected at bus 9. It is seen from Figs. 7.6 and 7.8, that although the reactive power consumption with 13 turbines is quite high, the voltage increases to the original value. This proves that the transmission capacity of the line is improved.

Grid strengthening may not be advisable beyond a certain level due to the following reasons:

(i) Strengthening the grid by reducing the impedance of transmission lines, leads to the use of many lines in parallel. This is not at all economical.
(ii) In this analysis, uncompensated WECS is assumed. In general, fixed capacitors are connected in parallel to the induction generators for reactive power compensation. Therefore, there is a danger of overcompensation if this method of grid strengthening is adopted.

Thus, the option of using different types of fixed reactive power compensation need to be studied.

7.6 Reactive Power Compensation

The reactive power compensation for WECS is traditionally done with capacitor banks, which is an economic and relatively simple solution. In order to avoid problems with over voltages, especially in island conditions, no-load compensation is most commonly used. No-load compensation means, that the compensation is designed to counterbalance the consumption of reactive power in the no-load situation, when the WECS operates at cut-in speed.

7.6.1 Shunt Compensation

Shunt (parallel) compensation is a common practice in WECS to improve the power factor of each turbine. Some WECSs use more than one capacitor bank at their terminals to compensate for reactive power at different wind speeds [20]. In case of a fixed shunt capacitor, the reactive power output of the capacitor is proportional to the square of the voltage across it. The reactive power required by the induction generator varies with operating slip. Thus with fixed shunt capacitor, the voltage varies with the slip of the induction generator and the number of turbines on-line.

The power flow analysis is carried out for different KVAR ratings of shunt capacitor compensation and with the grid strengthened using double circuit lines between PCC and the grid. A total of 5 wind turbines are assumed to be connected at bus 9. Simulation results are shown in Figs. 7.9, 7.10, 7.11 and 7.12. The uncompensated system is used as the base line. Figure 7.9 shows that the terminal voltage drops to 92 % when the system is uncompensated. With compensation, the voltage at WECS terminals is seen to be within the limit of ±5 % of rated value. Figure 7.10 shows that the reactive power demand reduces significantly. Figure 7.11 shows a reduction in line current with compensation. This proves that the advantage of an improved power factor is the reduction of total current, which,

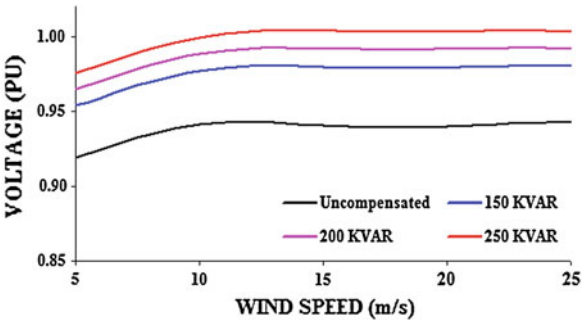

Fig. 7.9 Voltage at WECS terminals with various values of shunt compensation

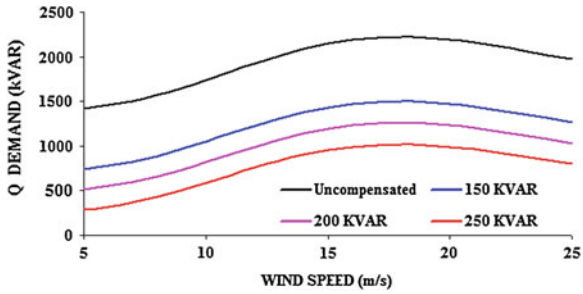

Fig. 7.10 Reactive power demand with various values of shunt compensation

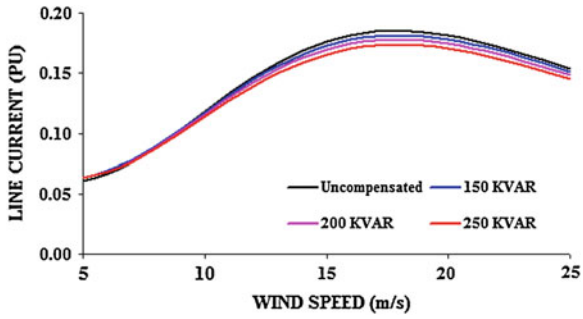

Fig. 7.11 Line current with various values of shunt compensation

in turn, reduces transmission loss and improves voltage regulation. This is also reflected in the PV curve of Fig. 7.12.

In order to study the effect of compensation in improving the number of turbines connected at bus 9, the power flow analysis is carried out for cut-in speed and for different ratings of shunt capacitor compensation. The results are shown in Figs. 7.13 and 7.14.

Figure 7.13 shows that with a compensation of 250 kVAR, an additional 12 turbines can be connected for the same transmission line (assuming that the thermal limit is not reached). Without shunt compensation, only 5 turbines can be connected.

Figure 7.14 shows that the slope of PQ curve reduces with compensation, reflecting the improvement in power factor.

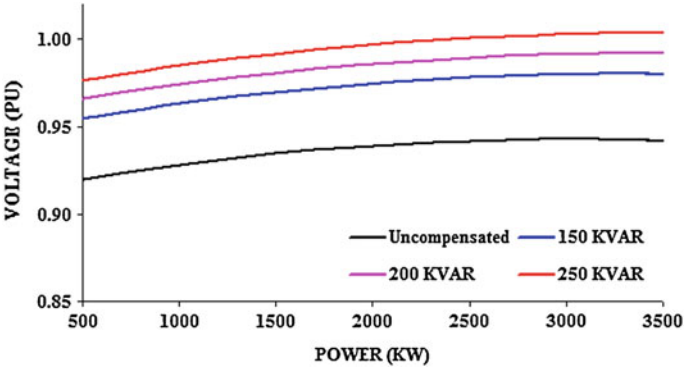

Fig. 7.12 Power generated versus voltage at WECS terminals with various values of shunt compensation

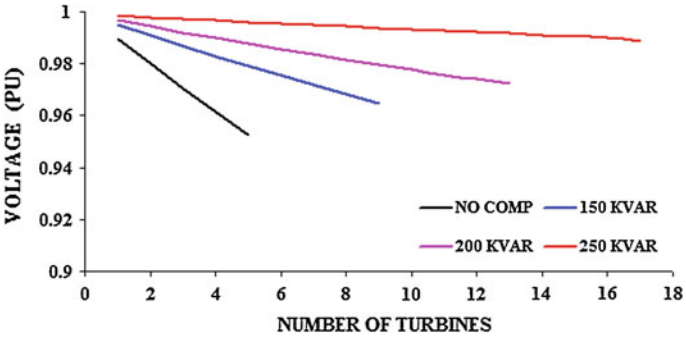

Fig. 7.13 Effect of increasing the number of turbines with shunt compensation—Voltage at WECS terminals

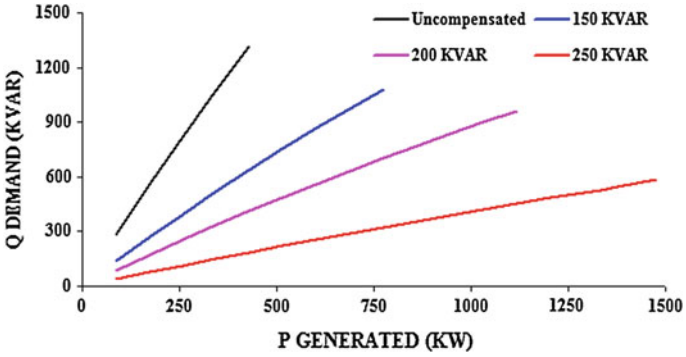

Fig. 7.14 Effect of increasing the number of turbines with shunt compensation—P Vs Q of WECS

7.6.2 Series Compensation

For the system shown in Fig. 7.2, the series capacitor is connected in the transmission line between the infinite bus and the PCC i.e., in the line between buses 4 and 5. The voltage across the series capacitor has a 180° phase shift with respect to the voltage drop across the line reactance. Thus, the voltage across the series capacitor will be used to counteract the voltage drop across the line impedance. Series capacitors are often used to improve the power transfer capability of transmission lines.

In order to study the effect of series compensation, the power flow analysis is carried out for cut-in speed and for different values of series capacitor reactance measured as a percentage of transmission line reactance. Series capacitor reactance equal to 25, 50 and 75 % of transmission line reactance are selected, because 100 % compensation for line reactance is not practically feasible. The maximum compensation is governed by sub-synchronous resonance and by series capacitor short-circuit overcurrent protection needs and it is generally about 80 % [21]. The results obtained are shown in Figs. 7.15 and 7.16. Figure 7.15 shows that with series capacitor reactance equal to that of 75 % of line reactance, 22 turbines can be connected with the same double circuit lines. With shunt compensation, only 17 turbines can be connected. Even with 50 % series compensation, 18 turbines can be installed. Thus series compensation becomes a cost effective alternative to transmission line strengthening. Figure 7.16 shows that the slope of the PQ curve does not significantly change with series compensation. In fact, there is a slight increase in slope with compensation. This proves that series compensation does not improve the power factor. But it helps to accommodate more turbines. From Figs. 7.15 and 7.16, it is clear that 25 % series compensation has no significant effect.

To see the effect of series compensation on the steady state improvement, in the entire wind speed range, simulation is carried out with 10 turbines on-line and for 50 and 75 % series compensation. Although, with series compensation more than 20 turbines can be connected, only 10 turbines is chosen for simulation, because as seen from Fig. 7.15, the voltage is reasonably within limits for 10 turbines. The results are shown in Figs. 7.17, 7.18, 7.19 and 7.20. It is observed from these Figures that with 10 turbines on-line, complete convergence over the entire wind speed range, from cut-in to cut-out speed, is achieved with series compensation. It is seen that without compensation, the power flow does not converge over the entire speed range considered. From Figs. 7.17 and 7.18 it is observed that there is power and voltage increase with compensation. Figure 7.19 shows that the reactive power demand at WECS terminals increases. From Fig. 7.20, it can be observed that the line current increases with series compensation in comparison to the uncompensated system. It is now clear that series compensation reduces the voltage drop across the transmission line, thus improving the voltage at WECS terminals and improving the power transferred. The power factor of the wind farm is not affected by series compensation.

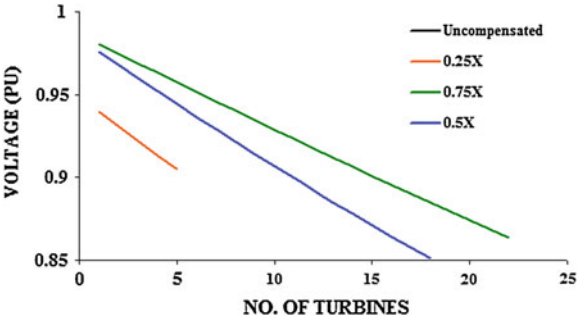

Fig. 7.15 Effect of increasing the number of turbines with series compensation—Voltage at WECS terminals

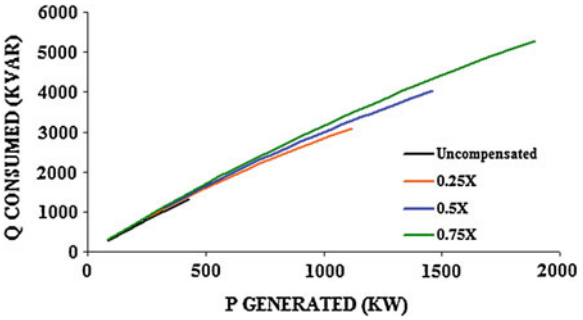

Fig. 7.16 Effect of increasing the number of turbines with series compensation—P Vs Q of WECS

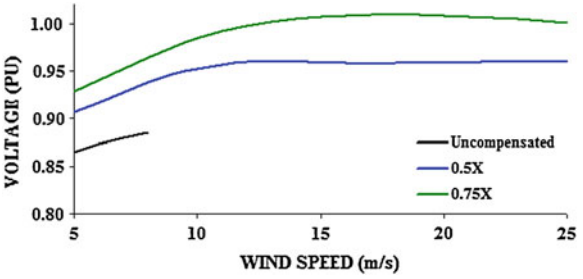

Fig. 7.17 Voltage at WECS terminals with various values of series compensation

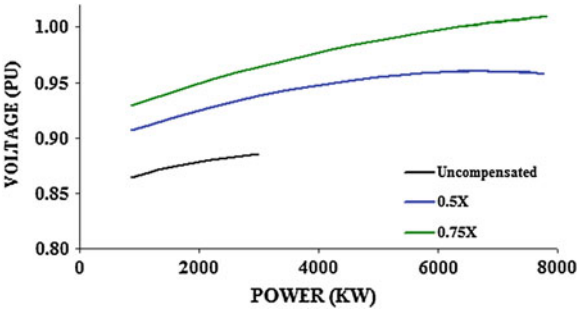

Fig. 7.18 Real power generated Vs voltage at WECS terminals with various values of series compensation

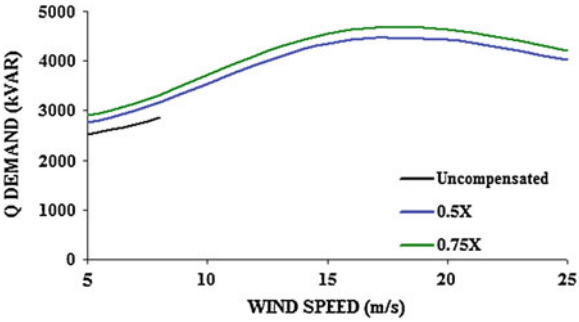

Fig. 7.19 Reactive power demand with various values of series compensation

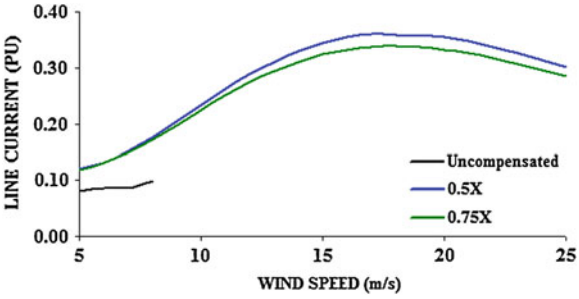

Fig. 7.20 Line current with various values of series compensation

7.6.3 Series-Shunt Compensation

It is clear from the above analysis, that the advantage of both shunt and series compensation of an AC capacitor can be made use of. In shunt compensation, the capacitor is used to compensate the individual induction generators. In series compensation, the capacitor is used to compensate the line impedance. The overall result will be an improvement in the voltage and lower losses on the transmission line.

To know the effect of the combined series and shunt compensations, simulations are carried out for two different combinations of series-shunt compensation. The same 10 wind turbines are connected at bus 9. Figure 7.21 illustrates the real power generated by WECS versus the voltage at the WECS terminals with various combinations of series-shunt compensations. It is seen that the voltage profile is high compared to individual series or shunt compensation. In fact, there is over compensation with series capacitor equal to 75 % of line reactance and shunt compensation of 200 kVAR.

Figure 7.22 shows that reactive power demand decreases significantly when compared to those with series compensation alone. As shown in Figs. 7.20 and 7.23, a comparison between the line current for series compensation and series-shunt compensation, it is observed that the transmission line current is reduced significantly with series-shunt compensation.

Comparing Figs. 7.12, 7.18 and 7.21, which show the variation of voltage with power for different types of compensation, it is evident that series-shunt

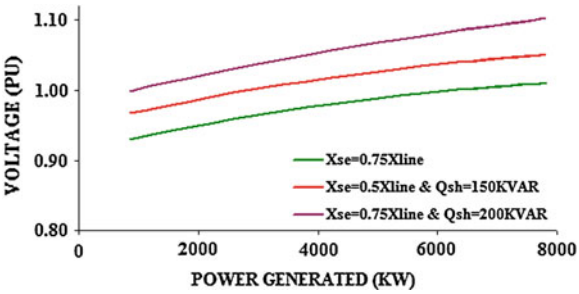

Fig. 7.21 Real power generated Vs voltage with series-shunt compensation

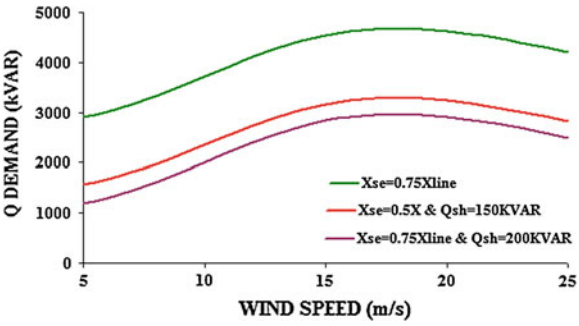

Fig. 7.22 Reactive power demand with series-shunt compensation

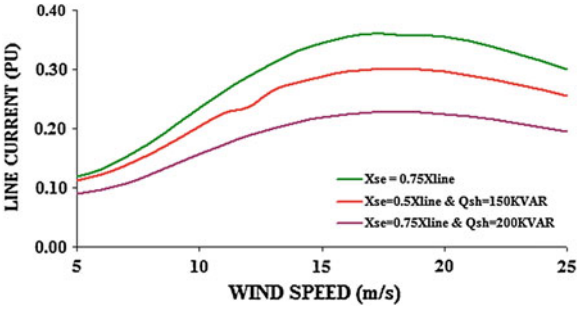

Fig. 7.23 Line current with series-shunt compensation

compensation provides a very good voltage profile at WECS terminals and increases the wind power penetration, as more turbines can be connected.

From Fig. 7.24, it is observed that series-shunt compensation with 50 % series compensation and 150 kVAR shunt compensation gives better voltage profile than that obtained by strengthening the grid with 5 parallel lines. Also, for such capacitor combination, the reactive power demand and transmission line current are reduced significantly as seen from Figs. 7.22 and 7.23. Thus it can be concluded that series-shunt compensation is an economical alternative to grid strengthening.

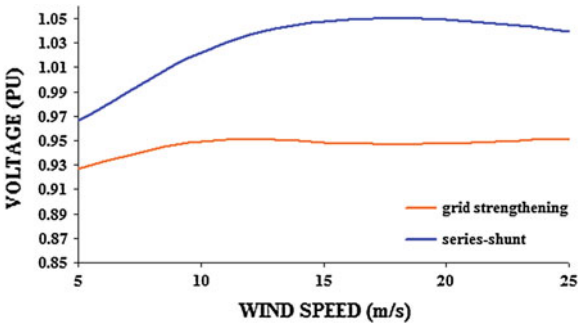

Fig. 7.24 Comparison of series-shunt compensation with grid strengthening

Table 7.2 Summary of results

	Max. no. of turbines that can be connected	V (PU)	P (MW)	Q (MVAR)	I (PU)
A1	2	0.9329	1.56	0.88	0.0735
A2	5	0.9389	3.89	2.21	0.1833
A3	13	0.9472	10.12	5.79	0.4325
B1	9	0.9788	3.89	1.49	0.1807
B2	13	0.9912	389	1.25	0.1771
B3	17	1.0031	3.89	1.01	0.1729
C1	18	0.9580	7.77	4.43	0.3604
C2	22	1.0090	7.77	4.68	0.3443
D1	13	1.0014	7.77	2.27	0.1782
D2	20	1.0619	7.77	1.91	0.1253

7.7 Discussion of Results

The convergence characteristics of the newly developed simultaneous method of power flow is compared with the existing sequential method of power flow analysis and it is found that the simultaneous method results in less number of iterations.

For the particular WECS modelled, the effect of increasing the number of turbines with and without compensation is summarized in Table 7.2. From Table 7.2 it is seen that when the transmission line between the PCC and the grid is strengthened (with 5 parallel lines), 13 turbines can be connected and thus more power can be fed into the grid. The voltage profile at the WECS terminals is also found to improve, although the reactive power drawn from the grid is very large. Yet such strengthening is not cost effective, being the equivalent of having 5 lines in parallel. Therefore, the effect of different types of compensation is studied.

Table 7.2 shows that with shunt compensation, there is improvement in voltage profile and decrease in the reactive power demand. The line current reduces

thereby reducing transmission losses. The net effect is an improvement in power factor. With series compensation, there is improvement in voltage profile, although there is increase in the reactive power demand. The line current drawn is comparatively large, yet more turbines can be connected on-line. The net effect is an improvement in real power penetration. With series-shunt compensation there is a considerable improvement in voltage profile. At the same time, the reactive power demand and the line current drawn are both reduced compared to series compensation alone and are comparable with shunt compensation. A combination of series compensation equal to 50 % of line reactance and shunt compensation of 150 kVAR, shows better performance as compared to either series or shunt compensation alone, for the 9-bus radial system considered. Thus with the correct choice of capacitor sizes, a combination of series and shunt compensation can be used to improve the overall system performance.

In Table 7.2, V—voltage at WECS terminals at rated speed, P—Real power generated at rated speed, Q—Reactive power demand at rated speed, I—Line current at rated speed, A—Uncompensated system (1—without line strengthening, 2—with double circuit line, 3—with 5 lines in parallel), B—Shunt Compensation (1–150, 2–200, 3–250 kVAR), V, P, Q and I values with 5 turbines on-line, C—Series Compensation (1–0.5 X_{line}, 2–0.75 X_{line})—V, P, Q and I values with 10 turbines on-line, D—Series-shunt Compensation (1–$X_{se} = 0.5\ X_{line}$ and $Q_{sh} = 150$ kVAR, 2–$X_{se} = 0.75\ X_{line}$ and $Q_{sh} = 200$ kVAR)—V, P, Q and I values with 10 turbines on-line.

To summarize, the following are recommended:

1. To strengthen the grid to evacuate the maximum power output from the wind farms, corresponding to installed rated capacity. This is to ensure harvesting of the wind power in the windy seasons.
2. To go in for appropriate value of series-shunt capacitor compensation with grid connected induction generators.

Appendix I

Data for 9-Bus Radial System

1. Transmission Line Data (All Lines)

Resistance	0.24 Ω/km
Reactance	0.48 Ω/km
Susceptance	2.80 μS/km
Length	20.0 km

Table A.1 Transformer data

Parameter	Load transformer data (all)	Step up transformer data (at the wind bus)	Feeding transformer data
Rated apparent power	0.63 MVA	1.0 MVA	25 MVA
Rated voltage of MV side	15 kV	15 kV	110 kV
Rated voltage of LV side	0.4 kV	0.69 kV	15 kV
Nominal short-circuit voltage	6 %	6 %	11 %
Copper loss at rated power	6 kW	13.58 kW	110 kW

2. Load Data (All Loads)

0.150 + j0.147 MVA

3. Coefficients of C_P—λ Curve

C_1	0.5
C_2	67.56
C_3	0.4
C_4	0
C_5	1.517
C_6	16.286
Gear box ratio	67.5

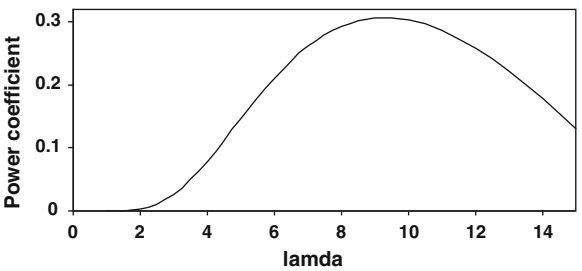

Fig. A.1 C_P—λ curve for the considered wind turbine

Asynchronous Generator Data (Δ-Connection)

Stator resistance	0.0034 Ω
Rotor resistance	0.003 Ω
Stator leakage reactance	0.055 Ω
Rotor leakage reactance	0.042 Ω
Magnetizing reactance	1.6 Ω

Appendix II

Jacobian Matrix for the 9-bus System

For the system considered the Jacobian is a (17 × 17) matrix as below. The numbers in the matrix represent the row and column of the elements. The analytical expressions for these elements are given in the subsequent sections.

$$\begin{bmatrix} (1,1) & \cdots & (1,8) & (1,9) & \cdots & (1,16) & (1,17) \\ \vdots & \ldots J_1 \ldots & \vdots & \vdots & \ldots J_2 \ldots & \vdots & \ldots J_5 \ldots \\ (8,1) & \cdots & (8,8) & (8,9) & \cdots & (8,16) & (8,17) \\ (9,1) & & (9,8) & (9,9) & & (9,16) & (9,17) \\ \vdots & \ldots J_3 \ldots & \vdots & \vdots & \ldots J_4 \ldots & \vdots & \ldots J_6 \ldots \\ (16,1) & & (16,8) & (16,9) & & (16,16) & (16,17) \\ (17,1) & \ldots J_7 \ldots & (17,8) & (17,9) & \ldots J_8 \ldots & (17,16) & (17,17) J_9 \end{bmatrix}$$

1 Elements of J_1

$$\frac{\partial P_i}{\partial \theta_i} = imag\left[\sum_{j \neq i} V_i^* V_j Y_{ij}\right]$$

$$\frac{\partial P_i}{\partial \theta_j} = -imag\left[\sum V_i^* V_j Y_{ij}\right]$$

2 Elements of J_2

$$\frac{\partial P_i}{\partial |V_i|}|V_i| = real\left[\sum_{j \neq i} V_i^* V_j Y_{ij}\right] + 2|V_i|^2 real\left(Y_{ij}\right)$$

$$\frac{\partial P_i}{\partial |V_j|}|V_j| = real\left[\sum V_i^* V_j Y_{ij}\right]$$

Diagonal element for WECS bus (bus 9),

$$J(8,16) = J(8,16) - \frac{2|V_9|^2 r_e}{(r_e^2 + x_e^2)}$$

3 Elements of J_3

$$\frac{\partial Q_i}{\partial \theta_i} = real\left[\sum_{j \neq i} V_i^* V_j Y_{ij}\right]$$

$$\frac{\partial Q_i}{\partial \theta_j} = -real\left[\sum V_i^* V_j Y_{ij}\right]$$

4 Elements of J_4

$$\frac{\partial Q_i}{\partial |V_i|}|V_i| = -imag\left[\sum_{j\neq i} V_i^* V_j Y_{ij}\right] - 2|V_i|^2 real(Y_{ij})$$

$$\frac{\partial Q_i}{\partial |V_j|}|V_j| = -imag\left[\sum V_i^* V_j Y_{ij}\right]$$

Diagonal element for WECS bus (bus 9),

$$J(16,16) = J(16,16) - \frac{2|V_9|^2 x_e}{(r_e^2 + x_e^2)}$$

$$\text{where}, Z_e = Z_S + Z_m||Z_r$$

5 Elements of J_5

$$J(8,17) = \frac{\partial}{\partial s}\left[\frac{V^2 r_e}{(r_e^2 + x_e^2)}\right] = \frac{|V_9|^2}{(r_e^2 + x_e^2)^2}\left[\left(x_e^2 - r_e^2\right)\frac{\partial r_e}{\partial s} - 2r_e x_e \frac{\partial x_e}{\partial s}\right]$$

6 Elements of J_6

$$J(16,17) = \frac{\partial}{\partial s}\left[\frac{-V^2 r_e}{(r_e^2 + x_e^2)}\right] = \frac{-|V_9|^2}{(r_e^2 + x_e^2)^2}\left[\left(r_e^2 - x_e^2\right)\frac{\partial x_e}{\partial s} - 2r_e x_e \frac{\partial r_e}{\partial s}\right]$$

7 Elements of J_7 : 0

8 Elements of J_8

$$J(17,16) = \frac{2|V_9| x_m^2 R_r / s}{\left[\left(R_1 + \frac{R_r}{s}\right)^2 + (x_1 + x_r)^2\right]\left[R_s^2 + (x_s + x_m)^2\right]}$$

$$\text{where}, Z_1 = Z_s||Z_m$$

9 Elements of J_9

$$J(17,17) = \frac{\partial \Delta P_m}{\partial s}$$

These are given by Eqs. (7.13) to (7.18).

References

1. Liangzhong Y, Phill C, Laurent S, Xiao-Ping Z (2005) Congestion management of transmission systems using FACTS. In: IEEE/PES transmission and distribution conference and exhibition, Asia and Pacific, Dalian, China, pp 1–5
2. Slootweg J, Polinder H, Kling W (2001) Initialization of wind turbine models in power system dynamics simulations. In: IEEE Porto power tech proceedings, p 7

3. Molzahn DK, Lesieutre BC (2013) Initializing dynamic power system simulations using eigenvalue formulations of the induction machine and power flow models. IEEE Trans Circuits Syst 60(3):690–702
4. Hatziargyriou D, Karakatsanis TS, Papadopoulos M (1993) Probablistic load flow in distribution systems containing wind power generation. IEEE Trans Power Syst 8(1):159–165
5. Persaud S, Fox B, Flynn D (2000) Impact of remotely connected wind turbines on steady state operation of radial distribution networks. IEE Proc Gener Transm Distrib 147(3):157–163
6. Meliopoulos APS (2001) Distributed energy sources: needs for analysis and design tools. In: IEEE power engineering society summer meeting, pp 548–550
7. Boulaxis NG, Papathanassiou SA, Papadopoulos MP (2002) Wind turbine effect on the voltage profile of distribution networks. Renewable Energy 25:401–415
8. Muljadi E, Wan Y, Butterfield CP, Parsons B (2002) Study of a wind farm power system. NREL report
9. Divya KC, Nagendra Rao PS (2005) Models for wind turbine generating systems and their application in load flow studies. Electr Power Syst Res 76:844–856
10. Fuerte-Esquivel CR, Acha E (1997) A Newton-type algorithm for the control of power flow in electrical power networks. IEEE Trans Power Syst 12:1474–1480
11. Liu Y, Wang W, Xu1 L, Ni P, Wang L (2008) Research on power flow algorithm for power system including wind farm. In: IEEE International Conference on Electrical Machines and Systems ICEMS, pp 2551–3255
12. Feijóo AE (2009). On PQ models for asynchronous wind turbines. IEEE Trans Power Syst 24(4):1890–1891
13. Feijoo AE, Cidras J (2000) Modeling of wind farms in the load flow analysis. IEEE Trans Power Syst 15(1):110–115
14. Pecas JA, Maciel FP, Cidras J (1991) Simulation of MV distribution networks with asynchronous local generation sources. In: Proceedings of IEEE Melecom
15. Cidras J, Martinez JA, Pecas JA, Maciel FP (1992) Modelling of nonlinear nodal admittances in load flow analysis. In: Proceedings IFAC
16. Salem E, Mohammed B, Joydeep M (2012) Power flow analysis of distribution systems with embedded induction generators. In: 44th North American power symposium, Sept 9–11, Illinois
17. EI-Sadek MZ, Dessauky MM, Mahmaud GA, Rashed WI (1997) Load representation for steady-state voltage stability studies. Electr Power Syst Res 43:187–195
18. Jayashri R, Kumudini Devi RP (2006) Analysis of the impact of interconnecting wind turbine generators to the utility grid. Wind Eng 30:303–315
19. Lubosny Z (2003) Wind turbine operation in electric power systems advanced modelling. Springer, Berlin
20. Chompoo-inwai C, Lee Wei-Jen, Fuangfoo Pradit, Williams Mitch, Liao James R (2005) System impact study for the interconnection of wind generation and utility system. IEEE Trans Ind Appl 41(1):163–168
21. Laughton MA, Warne DJ (2003) Electrical engineer's reference book, 16th edn. Elsevier, Oxford